2015

Modeling and Control of a Three-Port DC-DC Converter for PV-Battery Systems

Jianwu Zeng
University of Nebraska-Lincoln, jzeng@huskers.unl.edu

Wei Qiao
University of Nebraska-Lincoln, wqiao@engr.unl.edu

Liyan Qu
University of Nebraska-Lincoln, lqu2@unl.edu

Applied Power Electronics Conference and Exposition (APEC), 2015 IEEE
DOI: 10.1109/APEC.2015.7104586
Publication Year: 2015 , Page(s): 1768 - 1773

Modeling and Control of a Three-Port DC-DC Converter for PV-Battery Systems

Jianwu Zeng, *Student Member*, *IEEE*
Power and Energy Systems Laboratory
Deparment of ECE
University of Nebraska-Lincoln
Lincoln, NE 68588-0511, USA
jzeng@huskers.unl.edu

Wei Qiao, *Senior Member*, *IEEE*
Power and Energy Systems Laboratory
Deparment of ECE
University of Nebraska-Lincoln
Lincoln, NE 68588-0511, USA
wqiao@engr.unl.edu

Liyan Qu, *Member*, *IEEE*
Power and Energy Systems Laboratory
Deparment of ECE
University of Nebraska-Lincoln
Lincoln, NE 68588-0511, USA
lqu2@unl.edu

***Abstract*—This paper presents modeling and decoupled control design for an isolated three-port DC-DC converter (TPC), which interfaces a photovoltaic (PV) panel, a rechargeable battery, and an isolated load. A small signal model is derived from the state-space equations of the TPC. Based on the model, two decoupled controllers are designed to control the power flows of the two sources and the load voltage independently. Experimental studies are performed to verify that the two controllers are capable of regulating the power flows of the PV panel and the battery while maintaining a constant output voltage for the TPC.**

***Keywords*—Battery, decoupling control, three-port DC-DC converter, photovoltaic (PV).**

I. INTRODUCTION

It is expected that distributed renewable energy sources will be more and more used in the future electric grid. Power converters will play an important role in interfacing the renewable energy sources and the electric grid and load [1]. The power management and grid integration of multiple energy sources are commonly realized by using multiple individual converters. Compared to that solution, using an integrated multiport converter is preferable since it has less components and a higher power density [2]-[5]. Besides, it requires no communication capabilities that would be necessary for multiple individual converters.

Depending on their voltage levels, the renewable energy sources are usually connected to an electric grid or a load through a one-stage or a two-stage power converter system. For the applications where the voltage of the renewable energy source is low, an isolated multiport DC-DC converter is preferred to be used in a two-stage power converter system, as shown in Fig. 1. The isolated multiport DC-DC converter has multiple input ports for connecting different sources and multiple functions. It not only regulates the low-level DC voltages of the sources to a constant high level required by the inverter, but also can provide other important control functions, such as maximum power point tracking (MPPT), for the renewable energy sources.

This material is based upon work supported by the Federal Highway Administration under Agreement No. DTFH61-10-H-00003. Any opinions, findings, and conclusions or recommendations expressed in this publication are those of the authors and do not necessarily reflect the view of the Federal Highway Administration.

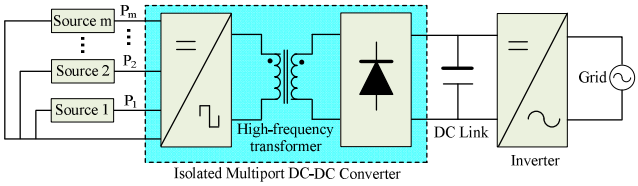

Fig. 1. Configuration of a two-stage, grid-connected, multisource energy system.

Due to the intermittence of the renewable energy sources, an energy storage device, such as a battery, is commonly used with the renewable energy sources. In such a hybrid energy system, a multiport converter with at least one bidirectional port, namely, a multiport bidirectional converter is required to interface the storage device. A variety of multiport bidirectional DC-DC converters has been proposed for two-stage grid integration of renewable energy sources [6]-[10]. These topologies either use too many active switches or have a negative effect on the battery lifetime due to the high-frequency charge/discharge for the battery. For example, in [10], the battery was both charged and discharged within a switching period. Such a high-frequency charge/discharge has a negative effect on the battery lifetime.

Recently, a new multiport bidirectional DC-DC converter with the least number of switches has been proposed [11]. In that converter, the battery was charged and discharged at a low frequency and the main switch could be turned off under the zero-current switching (ZCS) condition using a resonant circuit. However, the two switches in the bidirectional port are still hard switched. In this paper, an isolated three-port DC-DC converter (TPC) is proposed. Compared with the TPC in [11], the proposed TPC has the same number of the switch and all the switches can be turned on under the zero-voltage switching (ZVS) condition. Since a multiport converter is a multi-input multi-output (MIMO) system, a decoupling technique is desired to control different state variables of the system independently [6].

This paper presents a small signal model for the proposed TPC. Based on the model, two controllers are designed to regulate the power flows of the two sources and the output voltage of the TPC. Experimental results are provided to validate the proposed controllers when the TPC works in different conditions.

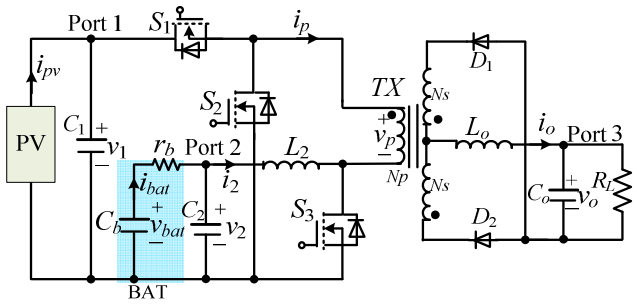

Fig. 2. The topology of the proposed TPC.

II. Topology and Operating Principle of the Proposed TPC

A. Topology of the Proposed TPC

Fig. 2 shows the topology of the proposed TPC. One input port consisting of a capacitor C_1 and two switches S_1 and S_2 is connected with a photovoltaic (PV) panel; the other input port consisting of a switch S_3, an inductor L_2, and a capacitor C_2 is connected with a battery. These two input ports are connected to the primary side of the high-frequency transformer whose turn ratio is defined as $n = N_p / N_s$, where N_p and N_s represent the numbers of turns of the primary and secondary windings, respectively. The output port consisting of two rectifier diodes D_1 and D_2, an inductor L_o and a capacitor C_o is connected to the load. The power flow of Port 2 is bidirectional such that the battery can work in both charging and discharging modes. As shown in Fig. 2, the battery is modeled as a capacitor C_b connected in series with its internal resistance r_b. The capacitance of C_b is sufficiently large such that v_{bat} is taken as a constant value during the modeling stage.

Define S_j^* the gate signal of the switch S_j (j = 1, 2, 3). When the switch S_j is on, S_j^* = 1; otherwise, S_j^* = 0. Fig. 3 shows the gate signals of the three switches and the voltage v_p across the primary side of the transformer. The switches S_1 and S_2 are switched complementarily with each other. According to the states of the three switches, the proposed TPC has three operating stages I, II, and III. The state

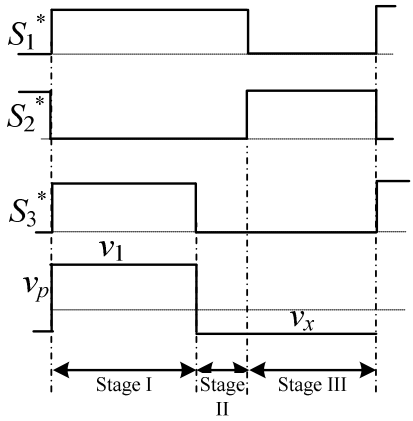

Fig. 3. The gate drive signals of the three switches and the voltage v_p across the primary side of the transformer.

variables include the voltages across the capacitors C_1, C_2, and C_o, and the currents through the inductors L_2 and L_o.

B. Operating Principle

In Stage I, S_1 and S_3 are turned on and S_2 is off; a positive voltage is applied to the primary side of the transformer, i.e., $v_p = v_1$; the renewable energy is directly delivered to the load side. This stage will not terminate until the switch S_3 is turned off. The differential equations in this stage can be expressed as follows

$$\begin{cases} i_{pv} = C_1 \dfrac{dv_1}{dt} + \dfrac{i_o}{n} \\ -v_2 = L_2 \dfrac{di_2}{dt} \\ C_2 \dfrac{dv_2}{dt} = \dfrac{v_{bat} - v_2}{r_b} - i_2 \\ i_o = C_o \dfrac{dv_o}{dt} + \dfrac{v_o}{R_L} \\ \dfrac{v_1}{n} - v_o = L_o \dfrac{di_o}{dt} \end{cases} \tag{1}$$

where i_{pv} represents the current of the PV panel and R_L represents the load resistance.

In stage II, S_3 is turned off and S_1 is turned on; the voltage across the primary side of the transformer is a negative v_x, i.e., $v_p = v_x$.

$$\begin{cases} i_{pv} = C_1 \dfrac{dv_1}{dt} - i_2 \\ (v_x + v_1) - v_2 = L_2 \dfrac{di_2}{dt} \\ C_2 \dfrac{dv_2}{dt} = \dfrac{v_{bat} - v_2}{r_b} - i_2 \\ i_o = C_o \dfrac{dv_o}{dt} + \dfrac{v_o}{R_L} \\ \dfrac{v_x}{n} - v_o = L_o \dfrac{di_o}{dt} \end{cases} \tag{2}$$

In Stage III, S_1 is turned off and S_2 is turned on; the voltage across the primary side of the transformer is the same as that in Stage II.

$$\begin{cases} i_{pv} = C_1 \dfrac{dv_1}{dt} \\ v_x - v_2 = L_2 \dfrac{di_2}{dt} \\ C_2 \dfrac{dv_2}{dt} = \dfrac{v_{bat} - v_2}{r_b} - i_2 \\ i_o = C_o \dfrac{dv_o}{dt} + \dfrac{v_o}{R} \\ \dfrac{v_x}{n} - v_o = L_o \dfrac{di_o}{dt} \end{cases} \tag{3}$$

According to the voltage second balance on the primary side of the transformer, v_x can be solved as follows

$$v_x = \frac{d_3}{1-d_3} \cdot v_1 \tag{4}$$

Then the average state-space model can be derived from (1)-(4)

$$\begin{cases} i_{pv} = C_1 \dfrac{dv_1}{dt} + \dfrac{i_o}{n} d_3 - i_2 (d_1 - d_3) \\ L_2 \dfrac{di_2}{dt} = v_2 - v_1 \cdot d_1 \\ C_2 \dfrac{dv_2}{dt} = \dfrac{v_{bat} - v_2}{r_b} - i_2 \\ C_o \dfrac{dv_o}{dt} = i_o - \dfrac{v_o}{R_L} \\ L_o \dfrac{di_o}{dt} = \dfrac{2v_1}{n} d_3 - v_o \end{cases} \tag{5}$$

The equilibrium points can be calculated by setting all of the time-derivative terms in (5) to be zero, then

$$v_1 \cdot d_1 = v_2 \tag{6}$$

$$v_o = \frac{2v_1}{n} d_3 \tag{7}$$

Equations (6) and (7) reveal that v_1 and v_o can be regulated by d_1 and d_3, respectively.

III. Modeling and Controller Design

A. The Control System Structure

The objective of controlling the TPC is to extract the maximum power from the PV panel while maintaining a constant voltage v_o on the load side. Fig. 4 shows the block diagram of the control system connected to the proposed converter. The control system consists of an MPPT controller and two voltage controllers: an input voltage controller (IVC) and an output voltage controller (OVC).

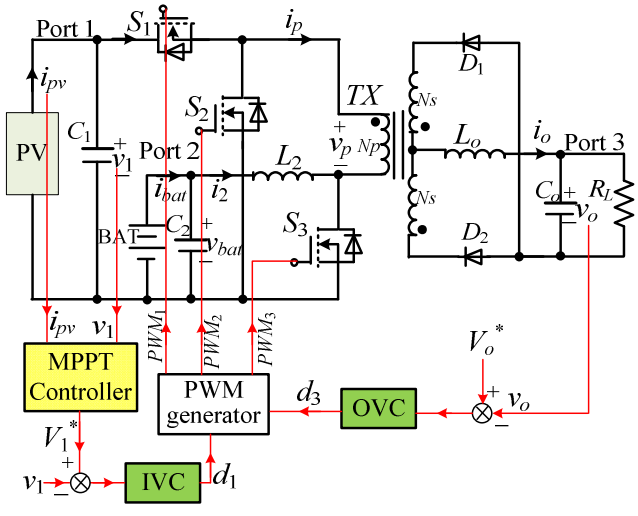

Fig. 4. Overall block diagram of the system with controllers.

The OVC is simply a voltage-mode controller, which takes the output voltage of the TPC, v_o, as the input and outputs the duty cycle d_3. The IVC is used to regulate the PV panel voltage to its reference voltage V_1^* obtained from a perturbation and observation MPPT controller [12]. The MPPT controller takes v_1 and i_{pv} as the input and outputs the desired V_1^*.

B. The Small-Signal Model of the TPC

The current and voltage of the PV panel has the following relationship

$$i_{pv} = I_{sc} - I_s \left(e^{\frac{v_1}{V_T}} - 1 \right) \approx I_{sc} - I_s e^{\frac{v_1}{V_T}} \tag{8}$$

where I_{sc} and I_s represent the short-circuit current and the reverse bias saturation current of the PV panel, respectively; V_T is the thermal voltage. Taking the first derivative of (8) yields

$$\hat{i}_{pv} = -\frac{I_s}{V_T} e^{\frac{V_1}{V_T}} \cdot \hat{v}_1 = \frac{1}{-r_{pv}} \cdot \hat{v}_1 \tag{9}$$

where $\hat{i}_{pv}$ and $\hat{v}_1$ represent the small signals of i_{pv} and v_1, respectively, and $-r_{pv}$ represents the equivalent resistance of the PV panel around a certain operating point specified by V_1. Then a small-signal model of the TPC which takes the form $\dot{x} = Ax + Bu$ is derived by using the state-space average method, where $x = [v_1, v_2, i_2, v_o, i_o]^T$ is the vector of state variables, $u = [d_1, d_3]^T$ is the vector of the outputs of the two voltage controllers,

$$A = \begin{bmatrix} \dfrac{-1}{r_{pv}C_1} & 0 & \dfrac{D_3 - D_1}{C_1} & 0 & -\dfrac{D_3}{nC_1} \\ 0 & \dfrac{-1}{r_b C_2} & \dfrac{-1}{C_2} & 0 & 0 \\ \dfrac{D_1}{L_2} & \dfrac{-1}{L_2} & 0 & 0 & 0 \\ 0 & 0 & 0 & -\dfrac{1}{R_L C_o} & \dfrac{1}{C_o} \\ \dfrac{2D_3}{nL_o} & 0 & 0 & -\dfrac{1}{L_o} & 0 \end{bmatrix},$$

and

$$B = \begin{bmatrix} \dfrac{-I_2}{C_1} & \dfrac{I_2 - I_o/n}{C_1} \\ 0 & 0 \\ \dfrac{V_1}{L_2} & 0 \\ 0 & 0 \\ 0 & \dfrac{2V_1}{nL_o} \end{bmatrix}$$

where D_1 and D_3 are the steady-state values of d_1 and d_3, respectively. Define $v(s) = [v_1(s), v_o(s)]^T$. Then, the transfer function is $v(s)/u(s) = G(s) = C\cdot[sE-A]^{-1}\cdot B$, where $C = [c_1, c_2]^T$, $c_1 = [1\ 0\ 0\ 0\ 0]^T$, $c_2 = [0\ 0\ 0\ 1\ 0]^T$, and E is an identity matrix, which has the same dimension as that of the matrix A. Then, $G(s)$ can be expressed as follows

$$G(s) = \begin{bmatrix} g_{11}(s) & g_{12}(s) \\ g_{21}(s) & g_{22}(s) \end{bmatrix} \tag{10}$$

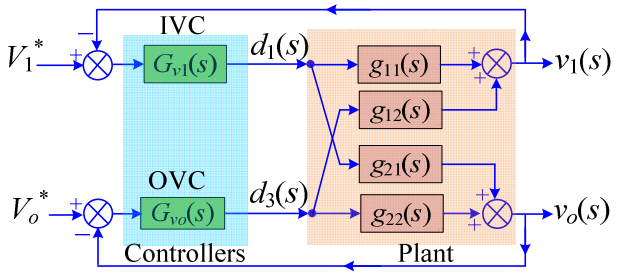

Fig. 5. Signal flows of the plant and the controllers.

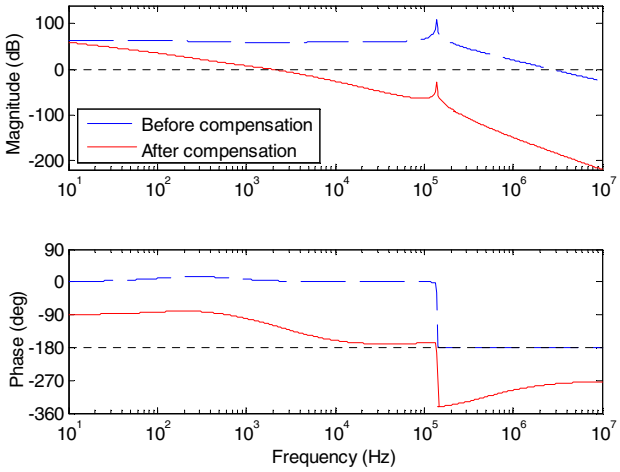

Fig. 6. Bode plots of $v_o(s)/d_3(s)$ before and after $G_{vo}(s)$ compensation.

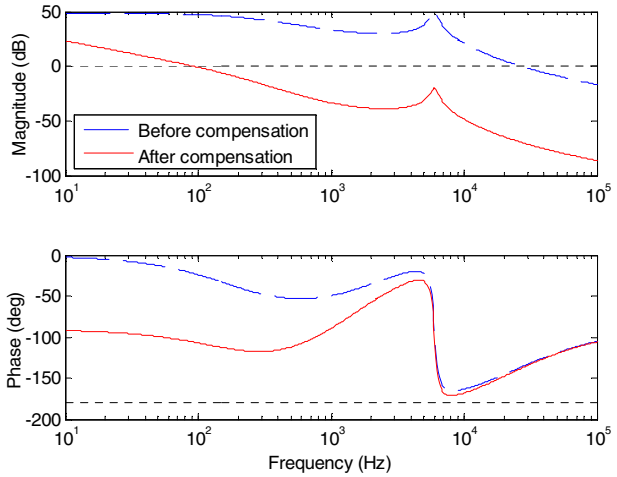

Fig. 7. Bode plots of $v_1(s)/d_1(s)$ before and after $G_{v1}(s)$ compensation.

C. Design of the Voltage Controllers

Fig. 5 shows the signal flows of the plant depicted by (10) as well as the two controllers $G_{v1}(s)$ and $G_{vo}(s)$. The plant is a multivariable system with the coupling terms $g_{12}(s)$ and $g_{21}(s)$, which require the two controllers, $G_{v1}(s)$ and $G_{vo}(s)$, to be properly designed and decoupled to control the input voltage v_1 and the output voltage v_o, respectively.

In this paper, the IVC loop is designed to have a bandwidth one decade lower than that of the OVC. In other words, d_1 can be assumed to be constant when designing $G_{vo}(s)$. Then the OVC is designed with the approximation that $v_o(s)/d_3(s) = g_{22}(s)$. Once $G_{vo}(s)$ is designed, the decoupled model for $v_1(s)/d_1(s)$ can be derived as follows:

$$\frac{v_1(s)}{d_1(s)} = g_{11}(s) - \frac{g_{12}(s)\cdot g_{21}(s)}{1+G_{vo}(s)\cdot g_{22}(s)}\cdot G_{vo}(s) \tag{11}$$

Then $G_{v1}(s)$ can be designed based on (11). The bode plots of $v_o(s)/d_3(s)$ and $v_1(s)/d_1(s)$ before and after $G_{vo}(s)$ and $G_{v1}(s)$compensations are plotted in Fig. 6 and Fig. 7, respectively. $G_{vo}(s)$ and $G_{v1}(s)$ are designed by choosing the cutoff frequencies of the OVC and IVC loops at 2 kHz and 100 Hz, respectively and suppressing the magnitudes of the closed-loop system transfer function at their corresponding resonant frequencies to be less than −20 dB. Then $G_{v1}(s)$ and $G_{vo}(s)$ can be derived as follows from the bode plots:

$$G_{v1}(s) = 0.8\cdot\left(0.0012 + \frac{1}{s}\right) \tag{12}$$

$$G_{vo}(s) = \frac{6\cdot\left(2\times10^{-6}s+1\right)}{s\left(3.1\times10^{-4}s+1\right)} \tag{13}$$

IV. Experimental Results

Fig. 8 shows the experimental setup of the whole system, where the TPC is connected with a BP XS3175 PV panel, a battery consisting of four PVX-3050T cells connected in series, a 700 Ω (R_L) resistive load, and an eZdsp F2812 control board on which the control algorithms are implemented. The open-circuit voltage (V_{oc}) and the short-circuit current (I_{sc}) of the PV panel are 43.2 V and 5.3 A, respectively. The nominal voltage and capacity of the battery are 24 V and 305 Ah,

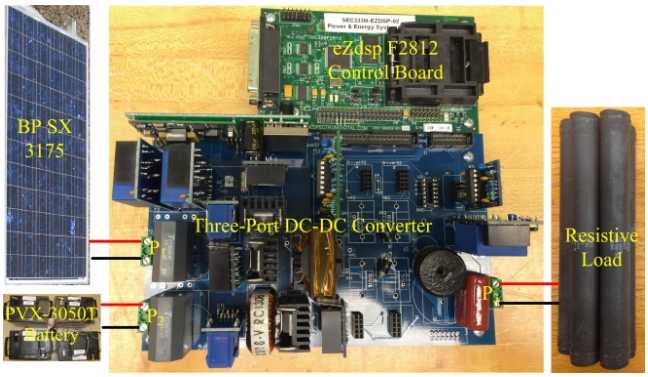

Fig. 8. The experimental system setup.

respectively; the switching frequency is 200 kHz. The reference output voltage (V_o^*) is 180V. To test the effectiveness of the IVC, the reference voltage of the PV panel (V_1^*) is simply set as 35 V. Other parameters of the experimental system are listed in Table I.

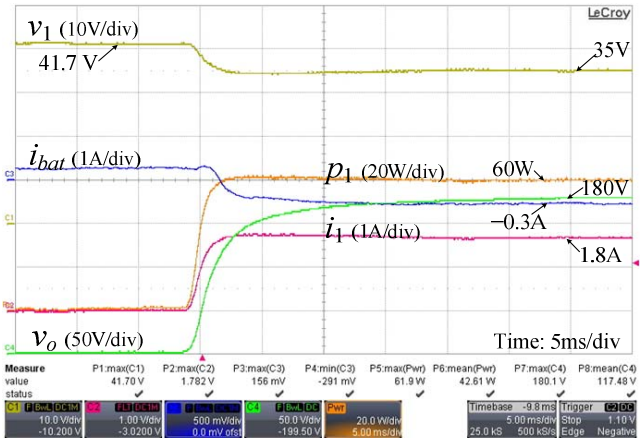

Fig. 9. Measured v_o and v_1 when the TPC starts.

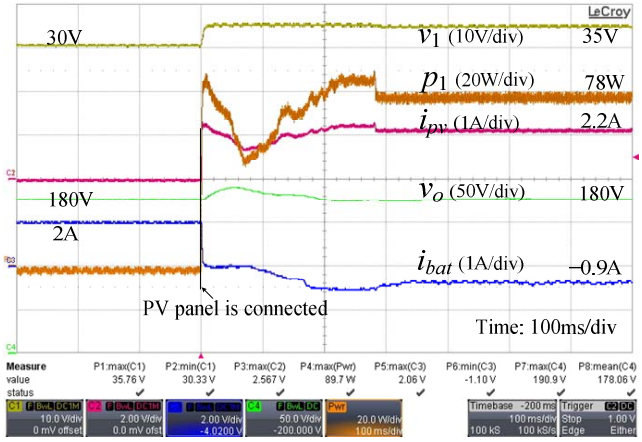

Fig. 10. Measured v_o and v_1 when the PV panel is connected to the TPC.

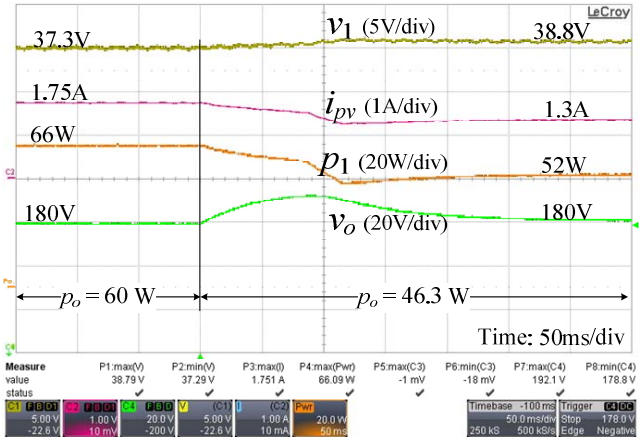

Fig. 11. Output voltage (v_o) response when the load is step changed.

TABLE I: PARAMETERS OF THE EXPERIMENTAL SYSTEM.

C_1, C_2	110 µF	C_o	220 µF
L_2	320 µH	L_o	18 µH
S_1, S_2	RFP12N10L	S_3	FDP3632
D_1, D_2	MUR440G	n	8:50

Fig. 9 shows the measured responses of v_o and v_1 when the TPC starts to work. Before that all of three switches are turned off. During the transient state, the voltage of the PV panel (v_1) decreases from its open-circuit voltage 41.7 V to 35 V. Meanwhile, v_o increases from zero to its reference value of 180 V. In the steady state, the power generated from the PV panel (p_1) is 60 W, which is higher than the load power 46.3 W. The surplus power is partly absorbed by the battery since its current is a negative value, i.e., $i_{bat} = -0.3$A.

Fig. 10 shows the measured responses of v_o and v_1 when the PV panel is connected to the TPC. The load is first supplied by the battery since the current of the PV panel is zero, i.e., $i_{pv} = 0$ A. Once the PV panel is suddenly connected to Port 1, i_{pv} increases such that the load is supplied by the PV panel. During the transient state, the output voltage of the TPC (v_o) first increases and then drops back to 180 V within 200 ms. Moreover, the voltage of the PV panel, v_1, is controlled at its reference value, which demonstrates the effectiveness of the IVC and OVC.

Fig. 11 shows the step response of the output voltage when the load is step changed from 60 W (R_L = 550 Ω) to 46.3 W. As shown in Fig. 11, the power generated from the PV panel (p_1) decreases from 66 W to 52 W during the transient; the output voltage (v_o) has a 11-V overshoot and then drops back to 180 V.

V. CONCLUSIONS

This paper has presented a small-signal model of a TPC for power management of a PV-battery system. Based on the model, an IVC and an OVC have been designed to regulate the voltage of the PV panel and the output voltage of the TPC, respectively. Experiments have been carried out to validate the two controllers. Results have shown that the voltage of the PV panel and the output voltage of the TPC could be well controlled by the two controllers independently.

REFERENCES

[1] H. Wu, R. Chen, J. Zhang, Y. Xing, H. Hu, and H. Ge, "A family of three-port half-bridge converters for a stand-alone renewable power system," *IEEE Trans. Power Electron.*, vol. 26, no. 9, pp. 2697-2706, Sept. 2011.

[2] C. Zhao, S. Round, and J. Kolar, "An isolated three-port bidirectional dc-dc converter with decoupled power flow management," *IEEE Trans. Power Electron.*, vol. 23, no. 5, pp. 2443-2453, Sept. 2008.

[3] J. Zeng, W. Qiao, L. Qu, and Y. Jiao, "An isolated multiport DC-DC converter for simultaneous power management of multiple different renewable energy sources," *IEEE J. Emerging Sel. Topics Power Electron.*, vol. 2, no. 1, pp. 70-78, Mar. 2014.

[4] J. Zeng, W. Qiao, and L. Qu, "An isolated multiport bidirectional DC-DC converter for PV-battery-DC microgrid applications," in *Proc. IEEE Energy Convers. Congr. Exposit.*, Sept. 2014, pp. 4978-4984.

[5] Z. Wang and H. Li, "Integrated MPPT and bidirectional battery charger for PV application using one multiphase interleaved three-port DC-DC

converter," in *Proc. IEEE Appl. Power Electron. Conf. Expo.*, Mar. 2011, pp. 295-300.

[6] H. Wu, K. Sun, R. Chen, H. Hu, and Y. Xing, "Full-bridge three-port converters with wide input voltage range for renewable power systems," *IEEE Trans. Power Electron.*, vol. 27, no. 9, pp. 3965-3974, Sept. 2012.

[7] Z. Ding, C. Yang, Z. Zhang, C. Wang, and S. Xie, "A novel soft-switching multiport bidirectional DC-DC converter for hybrid energy storage system," *IEEE Trans. Power Electron.*, vol. 29, no. 4, pp. 1595-1609, April 2014.

[8] K. Itoh, M. Ishigaki, N. Yanagizawa, S. Tomura, and T. Umeno, "Analysis and design of a multi-port converter using a magnetic coupling inductor technique," in *Proc. Energy Convers. Congr. Expo.*, Sept. 2013, pp. 4713-4718.

[9] Z. Qian, O. Abdel-Rahman, J. Reese, H. Al-Atrash, and I. Batarseh, "Dynamic analysis of three-port DC/DC converter for space applications," in *Proc. IEEE Appl. Power Electron. Conf. Exposit.*, Feb. 2009, pp. 28-34.

[10] Z. Qian, O. Abdel-Rahman, and I. Batarseh, "An integrated four-port DC/DC converter for renewable energy application," *IEEE Trans. Power Electron.*, vol. 25, no. 7, pp. 1877-1887, Jul. 2010.

[11] J. Zeng, W. Qiao, and L. Qu, "An isolated three-port bidirectional DC-DC converter for photovoltaic systems with energy storage," in *Proc. IEEE Ind. Appl. Soc. Annual Meeting*, Oct. 2013, pp. 1-8.

[12] C. Hua, J. Lin, and C. Shen, "Implementation of a DSP-controlled photovoltaic system with peak power tracking," *IEEE Trans. Ind. Electron.*, vol. 45, no. 1, pp. 99-107, Feb. 1998.